Ultrahigh Resolution X-ray Astronomy With Occulting Satellites: Phase I Final Report

P.I.: G. D. Starkman[1]; Co-I.: C. J. Copi[2]
Case Western Reserve University
Cleveland, OH 44106

Abstract

One of the challenges of X-ray astronomy is how to both collect large numbers of photons yet attain high angular resolution. Because X-ray telescopes utilize grazing optics, to collect more photons requires a larger acceptance angle which in turn compromises the angular resolution. All X-ray telescopes thus have angular resolution far poorer than their diffraction limit. Although collecting more photons is a desirable goal, sometimes selective collecting fewer photons may yield more information. Natural (such as lunar) occultations have long been used to study sources on small angular scales. But natural occulters are of limited utility because of their large angular velocities relative to the telescope, and because of the serendipity of their transits. In an earlier paper [6] and in the original Phase I proposal, we suggested that one might make use of a Steerable Occulting X-ray Satellite (*SOXS*) in conjunction with existing or planned X-ray telescopes to achieve very-high resolution of X-ray sources. In so doing we relied on analytic estimates of the binary point-source resolution. In this report, we repeat much of that background, and discuss the results of our Phase I investigation which shows that this technique would indeed work, not just for binary source resolution but to allow the high-resolution reconstruction of complex sources, such as real astronomical X-ray sources. This technique could therefore vastly improve the resolution of some future X-ray telescopes, particularly *Constellation X* where sub-milliarcsecond resolution is possible for a wide range of sources.

1 Introduction

One of the big challenges in doing X-ray astronomy is the relatively low photon fluxes from target sources. The fact that X-ray mirrors operate only at grazing angles of incidence further exacerbates this problem. Thus, while one might naively expect superb angular resolution from a $1.2\ \mathrm{m}$ aperture X-ray telescope such as the one on board the *Chandra* satellite, the 0.5 arcsecond reality is far from the 0.3 milliarcsecond nominal diffraction limit, and considerably worse than what is routinely achieved in longer wavelength bands. This situation is unlikely to change in the near future. Indeed, current plans for future X-ray missions opt for increased acceptance angle (and thus increased photon count rate) at the price of reduced angular resolution.

But it *is* possible to achieve higher X-ray photon count rates and yet improve one's angular resolution. The necessary step is to separate the collection of photons from the

[1] gds6@po.cwru.edu
[2] cjc5@po.cwru.edu

means of achieving high resolution. One way to do this is well-known—occultation. When an astronomical body, such as the moon, transits the field of view of a telescope, it occults different sources within the field of view at different times. By carefully measuring the photon count rate as a function of time during the transit, one can then reconstruct the projection of the surface brightness in the field of view onto the path of the occulter.

Natural occulters *have* been used to achieve high-resolution in X-ray observations; however, they have at least two distinct disadvantages:

1. Although natural occultations can be predicted, they cannot be scheduled—target sources are therefore limited, and multiple occultations of the same source over the course of a few years are uncommon.

2. Natural occulters have large angular velocities relative to a telescope. The shorter the transit time, the fewer photons one collects, and so the lower the resolution. This is especially important for X-ray astronomy, where photon count rates are relatively low.

There is however an alternative to natural occulters which can overcome both of these disadvantages—a steerable occulting satellite. Deployment of large steerable occulting satellites has been discussed for optical and near infra-red wavebands [1, 7, 4, 5], mostly for the purpose of finding planet around nearby stars, but also for high-resolution astronomical observations. However, such satellites are naturally well-suited for observations in the X-ray and far-UV. In the longer wavelength bands, minimization of diffractive losses pushes one to make the satellite as large as feasible, and deploy it as far as possible from the telescope. In the X-ray waveband one is far into the geometric optic limit and diffraction of the X-ray photons around the satellite can essentially be neglected; thus the optimal size and placement of the satellite are determined by one's ability to accurately position the satellite with respect to the telescope-star line-of-sight and to minimize the satellite's velocity perpendicular to that line-of-sight. The resolution delivered by the combination of the X-ray telescope and the *SOXS* is determined by the collecting area of the telescope (and thus the photon count rate for a source) and by the accuracy with which one can match the *SOXS* and telescope velocity. It is independent of the intrinsic resolution of the telescope.

For an X-ray telescope either at the L2 point of the Earth-Sun system (Constellation X) or in an eccentric high-Earth orbit (*Chandra* and *XMM*) we discuss in section 2 where to position *SOXS* relative to the satellite. In section 3 of this letter we discuss the X-ray blocking efficiency of a thick film and what it implies for the required thickness of the occulter. We also estimate in this section the required dimensions of an *SOXS*, which are determined mostly by limitations on telemetry. We discuss the steering of the *SOXS* in section 4. In section 5 we describe our image reconstruction technique and reconstruct some test sources. In section 6 we find the angular resolution that one obtains as a function of the *SOXS*–telescope relative angular velocity, and of photon count rate. In section 7 we discuss the the sky coverage that one could obtain in each

location. Application of these techniques to specific sources is discussed briefly in section 8. Finally, section 9 contains the conclusions.

2 Locating an *SOXS*

The location of an *SOXS* is dictated by the location of the telescope it is meant to occult. The *Chandra* X-ray telescope is in an elliptic orbit around the Earth with an apogee of $145,417$ km and a perigee of $16,026$ km. The *X-ray Multiple Mirror* (*XMM*) Telescope will also be inserted into an elliptic Earth orbit. Other X-ray telescopes, such as *Constellation X*, may be located at the second Lagrangian point of the Earth-Sun system. The orbital issues are entirely different for these two locations; we address each in turn below. Finally, some X-ray telescopes (*Astro-E* and *XEUS*) will be placed in low earth orbit. Because orbital velocities are so high in low earth orbit, it is more difficult to make use of the approach we advocate here; we will not discuss these further.

2.1 Orbit at L2

We have previously discussed the orbital advantages of placing a large occulter at L2 [5]. Here we will highlight the important points. Orbits around L2, both in the plane of the ecliptic and oscillations perpendicular to this plane, have periods of about 6 months independent of their distance from L2 (for distances $\lesssim 10^4$ km). Therefore the local gravity is very small. Both the total velocity and acceleration of orbits around L2 (relative to the L2 point) are on par with those we might attain through carefully tuning the orbit of *SOXS* relative to that of *Chandra* or *XMM*; the relative velocity of the satellite and telescope due to the motion of L2 about the Sun is of the same magnitude. If corrections are made to the *SOXS* orbit to cancel these then the acceleration perpendicular to the line-of-sight is about 5×10^{-10} m s^{-2}. Thus if the perpendicular velocity of *SOXS* relative to a particular line-of-sight between the telescope and some source is canceled by firing rockets, the perpendicular velocity will remain less than 10^{-4} m s^{-1} for at least a day. Tuning the velocity of *SOXS*, therefore, can be done very easily at L2.

2.2 Eccentric high Earth-orbit

As described above, the *Chandra* satellite is in an eccentric high altitude Earth orbit. The period of this orbit is 64 hours. The satellite therefore has an average angular velocity of about 6 arcseconds per second. An occulting satellite leading or following in *Chandra*'s orbit would transit a source at approximately that rate. The planned *X-ray Multiple Mirror Telescope* (*XMM*) has a similar orbit with a shorter 48 hour period. Given that the attainable angular resolution is related to the angular velocity of transit, the resolution that one could achieve with these orbits is minimal.

A great improvement is to place the *SOXS* in an orbit identical to that of the telescope but slightly modified by shifting the apogee and perigee, by changing the phase

of the satellite in the orbit, or by rotating the orbit. In all cases these modifications will put *SOXS* in an orbit with the same period as telescope. In such orbits the velocity perpendicular to the line of sight of *SOXS* and the telescope can be quite low. For example, consider placing *SOXS* in an orbit identical to that of the telescope (in terms of apogee, perigee, and orbital phase) but rotated about an axis through the centre of the Earth in the plane of the orbit and perpendicular to the line connecting apogee and perigee. The component of the relative velocity between *SOXS* and the telescope perpendicular to the line-of-sight between them is then zero throughout the entire orbit. Unfortunately, such an orbit intersects the telescope orbit at two points with disastrous consequences. The other orbital modifications mentioned above can alleviate this problem by enforcing a minimum separation of, for example, $10\ \mathrm{km}$ between the two spacecrafts. Although $10\ \mathrm{km}$ may seem fairly close, note that each spacecraft is only a few to tens of meters across; random errors therefore have a probability less than 10^{-9} per orbit crossing of causing catastrophic failure. The importance of utilizing these orbit modifications is explained more fully in sections 4 and 7.

3 Making an X-ray Occulter

3.1 Thickness

The attenuation length of X-ray photons in elemental matter is shown in figure 1. Except in hydrogen, it is approximately $3 \times 10^{-4}\ \mathrm{g\ cm^{-2}}$ at $1\ \mathrm{keV}$, and $10^{-2}\ \mathrm{g\ cm^{-2}}$ at $10\ \mathrm{keV}$. Thus a square $10\ \mathrm{m}$ on a side and one attenuation length thick has a mass of $0.3\ \mathrm{kg}$ at $1\ \mathrm{keV}$, and $10\ \mathrm{kg}$ at $10\ \mathrm{keV}$. At a typical density of $3\ \mathrm{g\ cm^{-3}}$, these represent thicknesses of just 1 micron and 30 microns respectively.

A useful occulter would need to be 3–5 attenuation lengths thick, and so 3–5 microns and 1–2 kg to operate at $1\ \mathrm{keV}$, and 100–150 microns and 30–50 kg to operate at $10\ \mathrm{keV}$. Even at $100\ \mathrm{keV}$ a $10\ \mathrm{m} \times 10\ \mathrm{m}$ lead film $0.6\ \mathrm{mm}$ thick at a mass of $600\ \mathrm{kg}$ would provide 3 attenuation lengths of occultation.

If positioning technology improved to the point where one could reduce the size of the occulter to 1–2 m, then even gamma ray occulters would be of reasonable mass.

3.2 Size

The size of the occulting satellite depend on two factors—the aperture of the telescope and the accuracy with which one can position the occulter.

The apertures of typical X-ray satellites are about $1\ \mathrm{m}$. This sets a lower bound on the dimensions of the occulter. Once the occulter is larger than the aperture of the X-ray telescope, there is essentially no effect on resolving power.

Next we will estimate how well we can determine the position of *SOXS* in the plane perpendicular to the telescope-source line-of-sight it is meant to occult. Consider a telescope separated from the *SOXS* by a distance r. We can mount a small diffraction-limited optical telescope of diameter d on the underside of the occulter. Using this

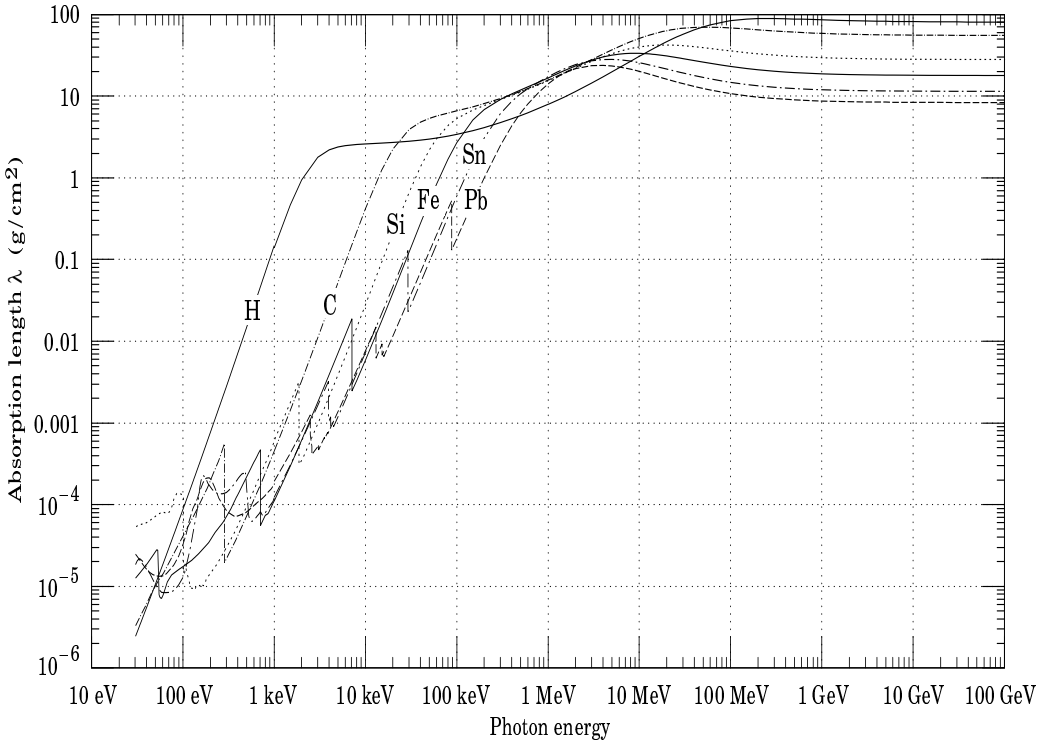

Figure 1: The photon mass attenuation length $\lambda = 1/(\mu/\rho)$ for various elemental absorbers as a function of photon energy (ρ is the density). The figure is obtained from the particle data book, figure 23.11 (http://pdg.lbl.gov). The data for $30\mathrm{eV} < E < 1\mathrm{keV}$ are obtained from http://www-cxro.lbl.gov/optical_constants (courtesy of Eric M. Gullikson, LBNL). The data for $1\mathrm{keV} < E < 100\mathrm{GeV}$ are from http://physics.nist.gov/PhysRefData, thru the courtesy of John H. Hubbel (NIST).

telescope we can establish the relative positions of the two satellite to within approximately

$$\delta x = 1.2 r \frac{\lambda}{d} = 0.5 \text{ m} \frac{r}{1000 \text{ km}} \frac{\lambda/400 \text{ nm}}{d/1 \text{ m}} \quad (1)$$

A 1 m positioning accuracy therefore requires a 50 cm finder scope at 1000 km separation, proportionately smaller at smaller separations. This is quite feasible, especially since the finder scope need not have a full UV plane.

An important question is whether one will collect enough photons to reach the diffraction limit of the angular resolution. There are two principal options—rely on reflected sunlight or shine a laser from the X-ray telescope onto the *SOXS* telescope. Collimation is not a significant problem, as seen by our calculation of the diffraction limit above. However, sunlight has an intensity of 1000 W m^{-2}, which will be difficult to match with a laser anyway. Assuming isotropic scattering from the telescope, and a total reflecting area of 1 m^2, this results in a flux at the *SOXS* of 3×10^8 s^{-1}, at 1000 km (falling as $1/r^2$). Detailed studies of existing telescopes (*Chandra*, *XMM*) would be required to precisely quantify our ability to locate the telescope relative to the *SOXS*, however, these estimates suggest that determining the relative position to within 1–3 m is not unrealistic. In the case of yet-to-be launched telescopes, the mounting of a small reflector on one or more corner of the telescope would be of definite benefit.

Although we have argued that we can determine the relative position of an *SOXS* and an X-ray telescope to within about a meter, we must also be able to reduce the velocity to a fraction of a meter per second. This can be done by a simple bootstrapping procedure. Two position determinations each with error of Δx, made a time t apart, determine the velocity within $\Delta v \simeq \sqrt{2}\Delta x/t$ (assuming the error in t to be negligible). If the relative velocity can be canceled within errors by accurately firing rockets, then the ability to reduce Δv is limited by the time one can allow between position determinations, $t = \Delta x/\Delta v$. This time is limited by the orbital accelerations, but is thousands of seconds for the elliptic earth orbits of interest (cf. subsection 7.2) and hundreds of thousands of seconds for orbits at L2. (cf. subsection 7.1). In practice it may be desirable to gradually reduce the relative velocity using repeated position determinations and rocket firings.

4 Steerability

In order to successfully resolve objects it will be necessary to frequently change the velocity of the satellite. These velocity changes will occur for two principal reasons: to move from one target source to another, and to match the velocity of the *SOXS* to that of the X-ray telescope. While solar radiation pressure might be used to some advantage, it will be necessary to make some velocity adjustments using rockets. The number and size of such adjustments may be the limiting factor on the useful lifetime of the *SOXS*.

A change Δv in the satellite's velocity is related by momentum conservation to the

mass of propellant ejected, $\Delta m_{\rm propellant}$, and the velocity of ejection $v_{\rm ejection}$:

$$\Delta v_{\rm sat} = \frac{\Delta m_{\rm propellant} v_{\rm ejection}}{m_{\rm sat}}. \tag{2}$$

If N is the number of desired major rocket-driven velocity changes, then we must keep $(\Delta m_{\rm propellant}/m_{\rm sat}) \leq N^{-1}$. (The mass of propellant ejected will of course vary on the particular maneuver, but here $\Delta m_{\rm propellant}$ is taken to be some typical mass of propellant expended per orbit reconfiguration.) We therefore can accommodate only a limited number of such rocket firings:

$$N \leq \frac{v_{\rm ejection}}{\Delta v_{\rm sat}}. \tag{3}$$

Off-the shelf, low-cost ion engines are currently available with ejection velocities of 20 km s^{-1}, and more expensive systems with 30 km s^{-1} performance have been developed, thus

$$N \leq \frac{30 \text{ km s}^{-1}}{\Delta v_{\rm sat}}. \tag{4}$$

Consider first the need to match the velocities of the two spacecraft so that a long occultation can occur. $\Delta v_{\rm sat}$ is then the relative velocity of the *SOXS* and the telescope in their orbits. In determining the sky coverage for elliptic Earth orbits in section 7.2 below we have considered only orbital configurations with relative velocities between the telescope and the *SOXS* of less than 10 m s^{-1}. (Near L2, the relative velocities of relevance are typically considerably smaller than that.) If $\Delta v_{\rm sat} \simeq 10$ m s^{-1}, then this implies $N \leq 3000$, which is a reasonable quota of corrections for a mission with a 3–5 year lifetime, given the typical 2–3 day orbital period of Earth-orbiting X-ray telescopes.

The second type of velocity correction that will be required is target acquisition—the readjustment of the orbit of the occulter so as to allow the occultation of a new target source. For satellites separated by 1000 km near L2, relative velocities are only $v_{\rm sat} = \mathcal{O}(10^{-4}$ km s$^{-1})$, and the expression for N (equation 4) shows that any constraint on target choice or order does not come from concerns about conserving propellant. For telescopes in orbit about the Earth, the matter is quite different. Here orbital velocities are $v_{\rm sat} = \mathcal{O}(1$ km s$^{-1})$, and so it is clear from the allowed number of orbital corrections (4) that one cannot indiscriminately rocket from one target to another on the sky. One solution might have been to sail in the solar radiation pressure. However, the solar radiation pressure is approximately $P_{\rm solar} = 6 \times 10^{-6}$ Pa. For an areal density of just 1.5×10^{-3} g cm^{-2} (five attenuation lengths as 1 keV), this results in an acceleration of only 4×10^{-4} m s^{-2}. At this rate it takes about a month to change velocity by 1 km s^{-1}.

Clearly one cannot reposition randomly on the sky. However the velocity difference between two orbits which result in occultation of target sources one degree apart are only of order 15 m s^{-1}. Solar sailing can cause velocity changes of this order in under a day. Moreover, the allowed number of orbital corrections (4) indicates that

rocket driven corrections of this magnitude can be made of order 1000 times. How many corrections we can make, and how many sources we can therefore target for occultation, clearly depends on exactly how we use the satellite. A reasonable program of observations certainly seems possible.

5 Image Reconstruction

This section represents the bulk of the new results from our Phase I study. A number of techniques have been applied to the problem of image reconstruction from lunar and asteroid eclipses. In the case of x-ray diffraction we operate in the geometric optics limit meaning that the light curve is easy to calculate but also lacks diffraction peaks that could further aid in the reconstruction process. We have implemented a reconstruction technique based on the eclipse mapping method (EMM) [2, 3]. EMM is a maximum entropy technique thus it can oversmooth the image or introduce spurious sources depending on the weighting between the entropy and the constraints.

We have implemented an improved EMM algorithm [3]. Briefly, we maximize the quality function

$$Q = S - \frac{\left[C(\chi^2)\right]^2}{\rho} - \frac{\left[C(R)\right]^2}{\rho^2}, \tag{5}$$

where S is the entropy, the usual least squares fit definition of χ^2 is used, $C(x) = (x - x_{\rm aim})/x_{\rm aim}$ and

$$R = \frac{1}{\sqrt{M-1}} \sum_{j=1}^{M-1} r_j r_{j+1} \tag{6}$$

is a measure of the correlations in the residuals. The parameter ρ controls the weighting between the entropy and the constraints. We start with a large value of ρ ($\rho \approx 100$) and anneal to a small value ($\rho \approx 10^{-4}$). This should allow the entropy to initially smooth the image then allow the constraints to sharpen the important features as we anneal. In practice we still tend to oversmooth the image which leads to a conservative estimate of the attainable resolution.

For our case we made an important modification to the EMM algorithm. Since we are in the geometric optics limit there are sharp transitions from an unocculted to a partially occulted to a fully occulted source. Thus sources only contribute to changes in the lightcurve while they are being occulted. We include this in our fit by giving more weight to the pixels that are causing the light curve to change and averaging over the effects from the rest of the pixels. A minimum pixel intensity is chosen; pixels above the minimum count fully in the fit while those below the minimum are averaged over. Again we start with a high value for this intensity and anneal to a low value.

To start the reconstruction we could use a low resolution image taken by the telescope without the presence of *SOXS*. For the test cases considered here we do not do this. Instead we bootstrap by initially performing a non-negative least squares fit. Since this is an underdetermined problem we do not get an unique solution. In fact, most of

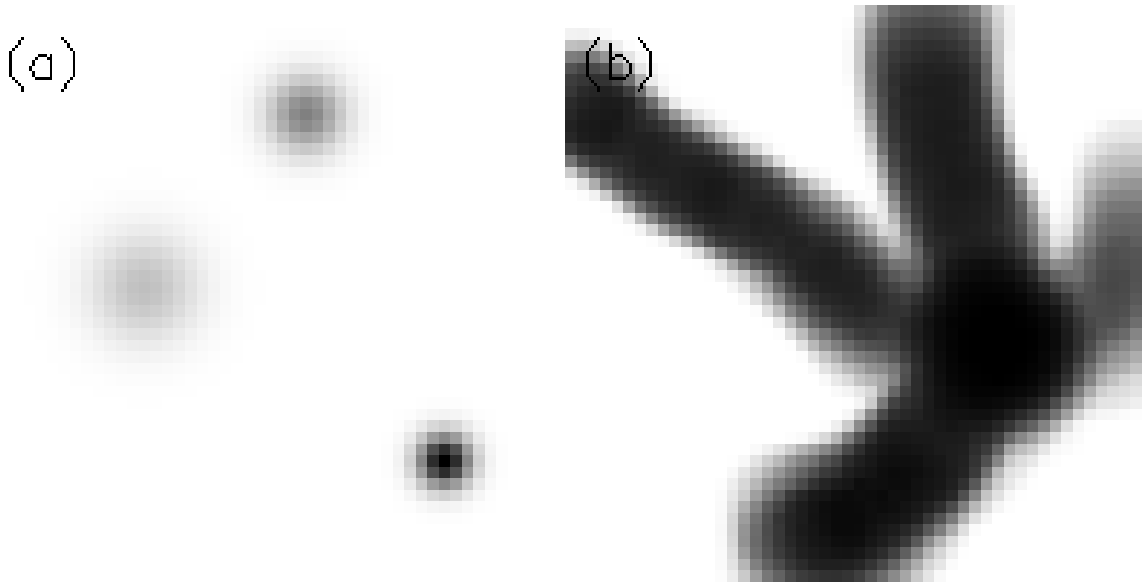

Figure 2: Image reconstruction test sources. (a) Three Gaussians with equal integrated intensities and peak intensities in a $4:2:1$ ratio. (b) Filaments radiating from a bright spot. Each image is 50×50 pixels.

the signal is typically placed in a few very bright pixels. To speed up the convergence of the reconstruction we presmooth the image with a Gaussian. The smoothing scale must be chosen with some care since oversmoothing doesn't help convergence either. Smoothing on the scale of a few pixels worked well for our test cases.

Two test cases have been considered (figure 2). The first contains three Gaussian sources. Each source has the same integrated intensity and widths chosen so that the peak intensities are in a $4:2:1$ ratio. The second contains filamentary structures radiating from a bright spot.

The reconstructions are performed for $10^3\gamma/\mathrm{snapshot}$ (figures 3, 5) and for $10^4\gamma/\mathrm{snapshot}$ (figures 4, 6). The satellite moves 1 pixel per snapshot. The simple geometry of the satellite provides information along only 1 direction for each pass over the source. Thus we consider (a) 2, (b) 4, (c) 8, and (d) 16 passes for each reconstruction. To extract maximal information from N passes the satellite travels along a path with an angle $\theta = \pi/N$ relative to the previous pass.

For the Gaussian source (figures 3 and 4) the reconstructions are, in general, oversmoothed. Too much of the intensity is spread throughout the image. In both cases 2 passes (a) show the existence of multiple sources but is not sufficient to resolve them. By 4 passes (b) we can resolve at least two sources. With 8 and 16 passes (c and d) all three sources can be resolved.

For the filamentary source (figures 5 and 6) the reconstructions do a good for the

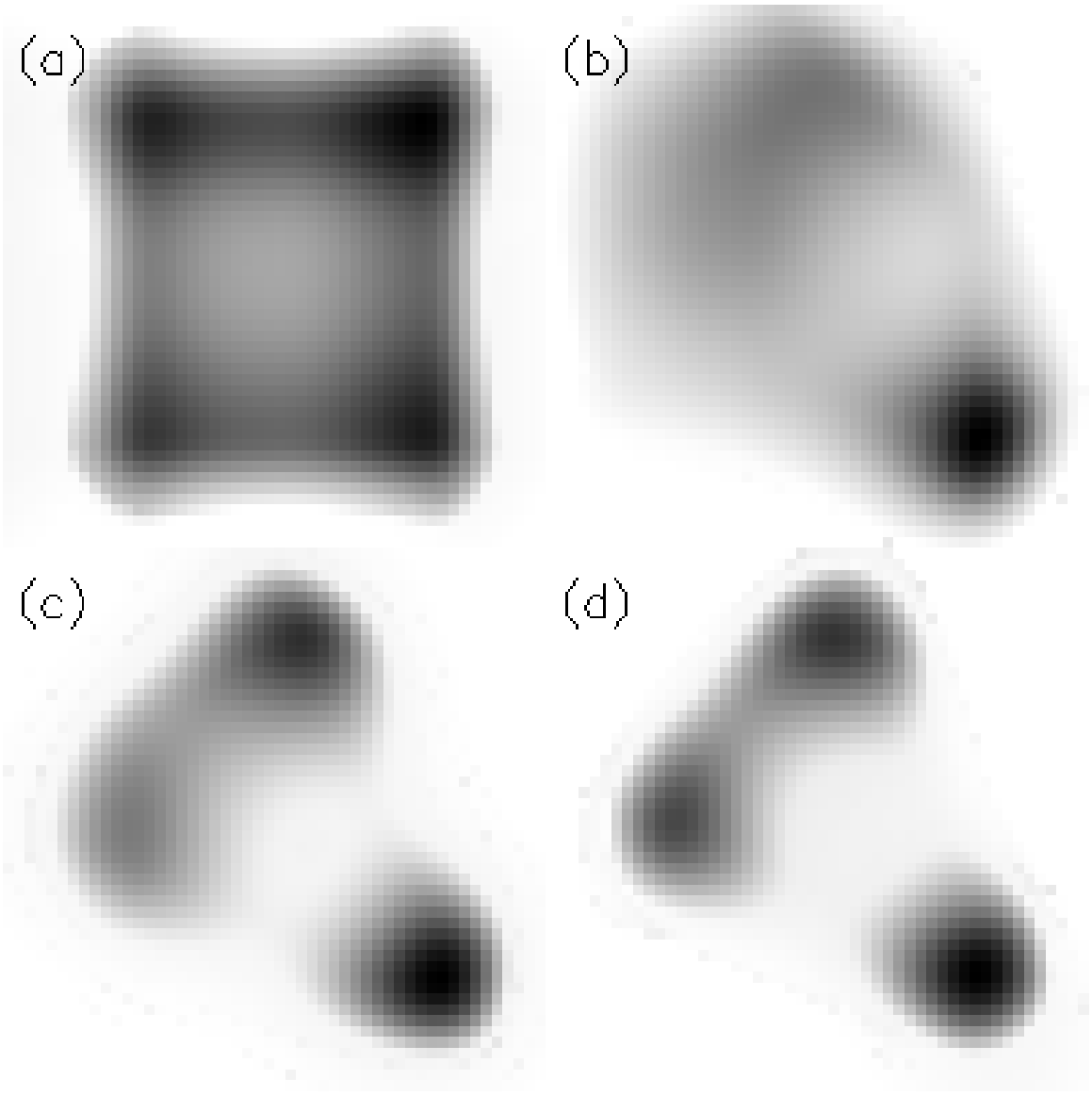

Figure 3: Reconstructed image for the Gaussian test source (figure 2(a)) with a $10^3\gamma/\mathrm{snapshot}$ total intensity. The reconstruction was performed for (a) 2, (b) 4, (c) 8, and (d) 16 passes as described in the text. The scale ranges from 0 to $20\gamma/\mathrm{snapshot}$ (minimum to maximum in the original source). Notice that reconstructed sources are oversmoothed.

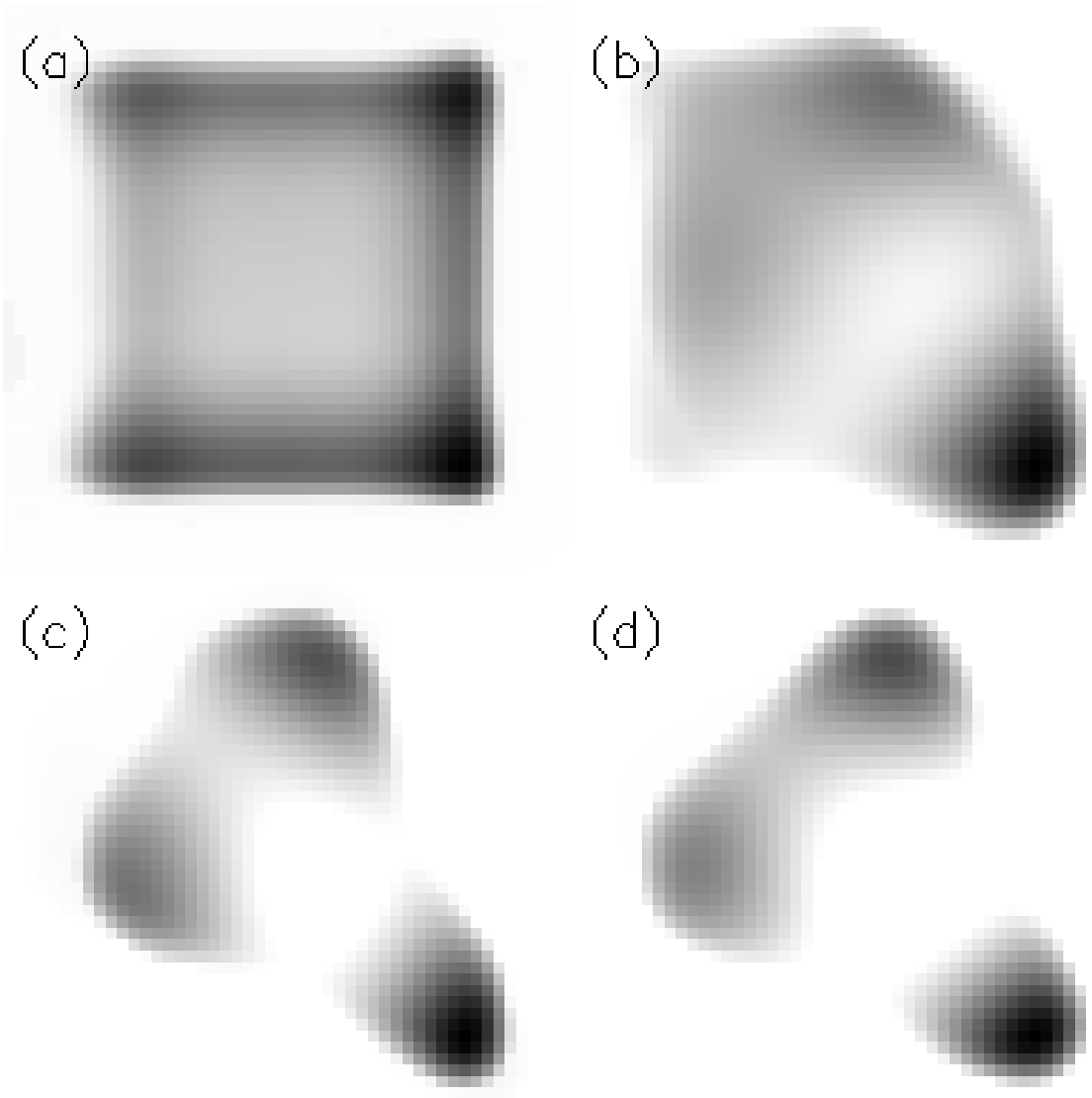

Figure 4: Reconstructed image for the Gaussian test source (figure 2(a)) as in figure 3 with a $10^4\gamma/\mathrm{snapshot}$ total intensity. The scale ranges from 0 to $200\gamma/\mathrm{snapshot}$.

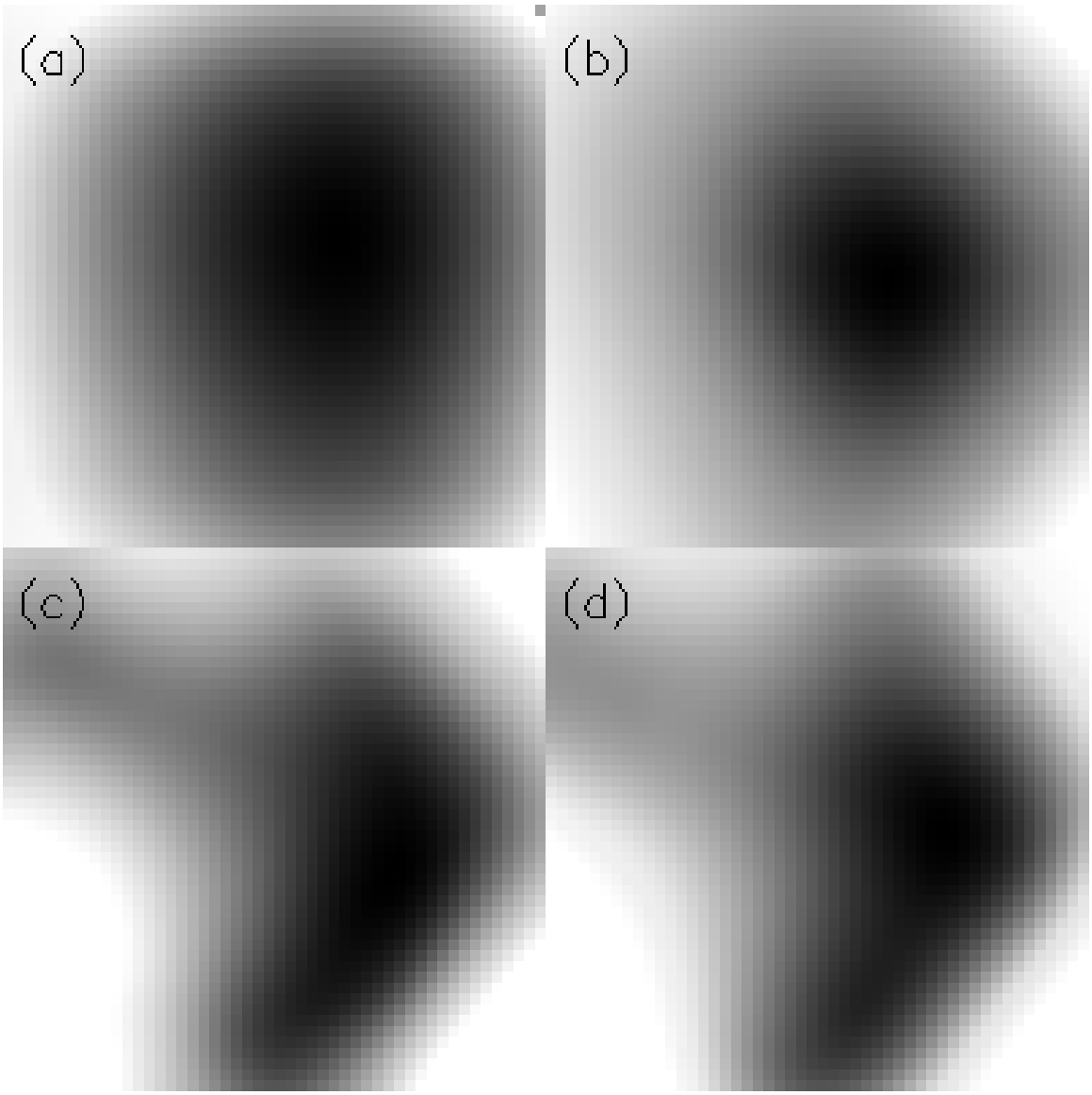

Figure 5: Reconstructed image for the filamentary test source (figure 2(b)) with a $10^3\gamma/\mathrm{snapshot}$ total intensity. The reconstruction was performed for (a) 2, (b) 4, (c) 8, and (d) 16 passes as described in the text. The scale ranges from 0 to $1.07\gamma/\mathrm{snapshot}$ (minimum to maximum in the original source).

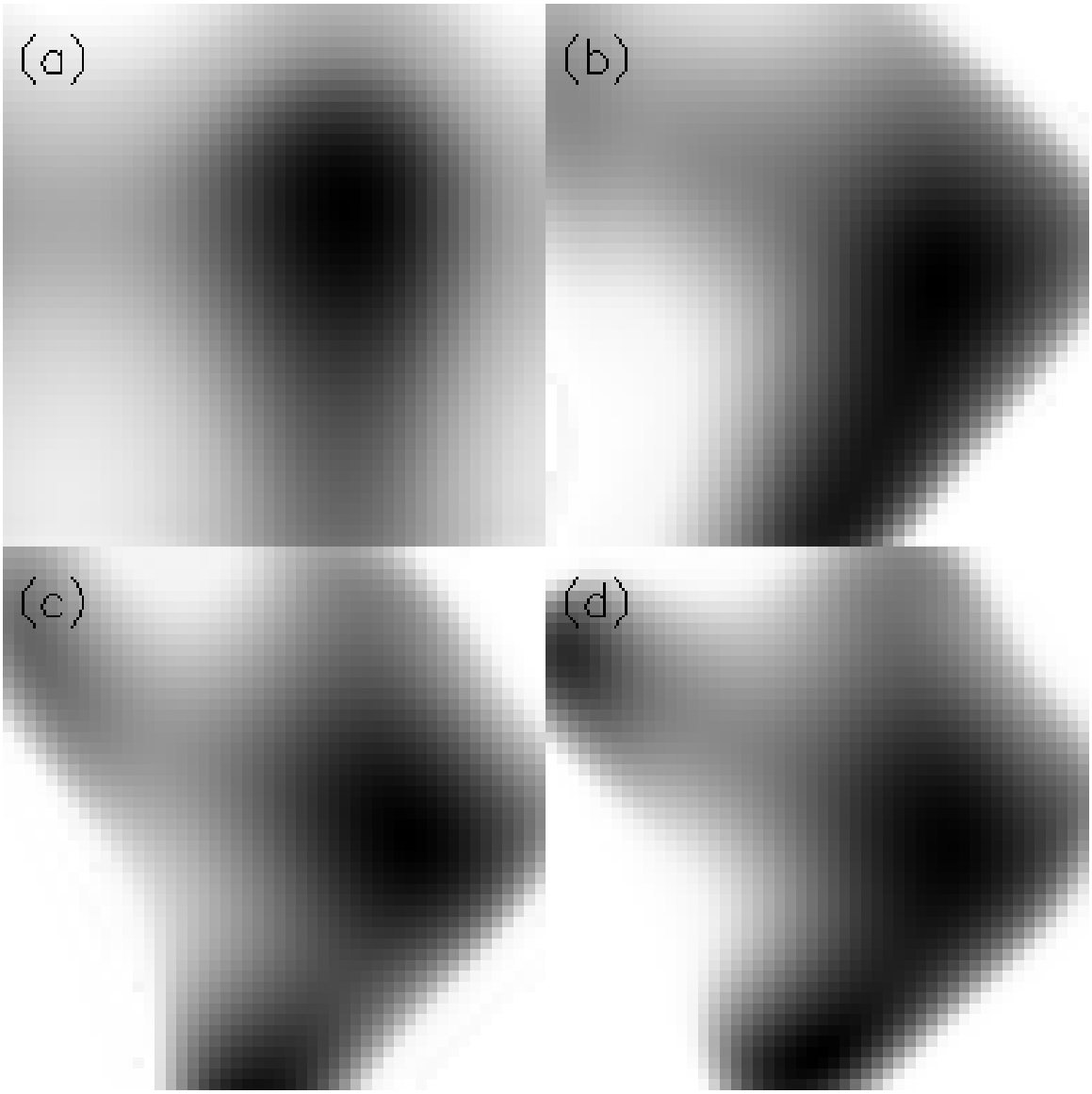

Figure 6: Reconstructed image for the filamentary test source (figure 2(b)) as in figure 5 with a $10^4\gamma/\mathrm{snapshot}$ total intensity. The scale ranges from 0 to $10.7\gamma/\mathrm{snapshot}$.

bright spot. In both the 8 and 16 passes (c and d) cases the filaments are resolved. For the brighter source the filaments are partially resolved with 4 passes (b) and a suggestion of filaments exists even with just 2 passes (a). Notice that even though the reconstruction technique involves Gaussian smoothing non-Gaussian structures can be resolved.

6 Resolution

When used in conjunction with an *SOXS* the telescope acts as a light bucket. The angular resolution of the telescope itself is irrelevant; instead the collecting area is the important telescope parameter. The angular resolution of the system will come from probing the lightcurve as *SOXS* transits a source.

To study the angular resolution of *SOXS* we consider the simple case of identifying a binary source. Let $f(\vec{x},t)$ be the normalized lightcurve (number of photons detected per second) generated as *SOXS* scans across a single source at a position $\vec{x}$ in the plane of *SOXS*. The lightcurve is the number of photons detected as a function of time. It is normalized such that the value is one (in the detector) when *SOXS* is not present. Since X-rays have extremely short wavelengths we can approximate the diffraction pattern produced by the satellite simply by the geometric shadow projected on the telescope. This reduces the lightcurve to a calculation of the area of the telescope not under the shadow of the occulter. We write the lightcurve of a single source as

$$l_1(\vec{x},t) = I_1 f(\vec{x},t) \tag{7}$$

and the total lightcurve for two sources at $\vec{x}_1$ and $\vec{x}_2$ can be written as

$$l_2(\vec{x}_1,\vec{x}_2,t) = I_2\left[\rho f(\vec{x}_1,t) + (1-\rho) f(\vec{x}_2,t)\right]. \tag{8}$$

Here I_i is the total intensity of the system for $i = 1$ or 2 sources and ρ is the intensity ratio of the two sources. We would like to find the minimum separation of two sources that can be distinguished from a single source. An observation consists of a sequence $\{O_j(\vec{x})/j = 1,...,n\}$ of measurements of the integrated lightcurve between times t_{j-1} and t_j:

$$O_j(\vec{x}) = \int_{t_{j-1}}^{t_j} dt\; l_i(\vec{x},t). \tag{9}$$

To obtain limits on the minimum separation we first evaluate the number of photons expected between time t_0 and t_k

$$L_{i,k}(\vec{x}) \equiv \int_{t_0}^{t_k} dt\; l_i(\vec{x},t) = \sum_{j=1}^{k} O_j(\vec{x}) \tag{10}$$

where i is 1 or 2 as above. Assuming the counts in each time bin, $[t_{j-1}, t_j)$, are Poisson distributed the likelihood of a model with i sources given an underlying model with 2

sources is

$$\mathcal{L}_i = \prod_{k=1}^{N} e^{-L_{i,k}} \left(L_{i,k}\right)^{L_{2,k}} \Big/ \left(L_{2,k}\right)!. \tag{11}$$

Finally the quantity

$$T = -2 \log \left(\frac{\mathcal{L}_1}{\mathcal{L}_2} \right) \tag{12}$$

is χ^2 distributed with 4 degrees of freedom (t_0, $x_2 - x_1$, I, and ρ) and allows us to calculate the probability of misidentifying a binary source as a single source. This probability depends on $\mu_\perp$, the angular velocity of *SOXS* as it transits the source. The results for the 95 percent confidence limits as a function of the intensity in a 1.2 m aperture telescope for $\rho = 1$, $1/3$, and $1/10$ and for $\mu_\perp = 10$ mas s^{-1}, $\mu_\perp = 1$ mas s^{-1}, and 0.1 mas s^{-1} are shown in figure 7. In producing figure 7 we assumed a uniform response over the surface of the telescope. A more complicated response function may improve resolution slightly.

The simple analysis employed here uses the edges of *SOXS* in a single occultation. In practice it would be necessary to obtain multiple projections to resolve a source in two dimensions. This could be facilitated by putting slits at various angles in *SOXS* that allow for sources to be occulted by different regions of the satellite in different ways during a single transit.

7 Sky Coverage

The issues of resolution and sky coverage are closely related. Here sky coverage is the fraction of the sky for which a particular angular resolution can be obtained. While one can reposition *SOXS* to be in an arbitrary direction on the sky relative to the X-ray telescope, this frequently leads to large relative velocities and accelerations between the occulter and telescope perpendicular to the line-of-sight, thus leading to poor resolution (see figure 7). Conversely, extremely good resolution is possible if the relative velocity during the occultation is kept quite low; however this requires either special orbits (and thus very little sky coverage) or expenditures of fuel. Here we will explore the sky coverage that can be obtained subject to a number of constraints.

7.1 L2 Orbits

As discussed above (section 2.1) the orbits at L2 are much simpler to manage than orbits around the Earth. Full sky coverage can be obtained and the velocity perpendicular to the line-of-sight can be chosen as desired. Figure 7 best represents what can be achieved at L2. Since the perpendicular velocity can be chosen, extremely high angular resolution is possible. Even sub-milliarcsecond resolution is possible for many sources ($\Gamma \gtrsim 4 \times 10^3$ s^{-1}) when $\mu_\perp = 0.1$ mas s^{-1}.

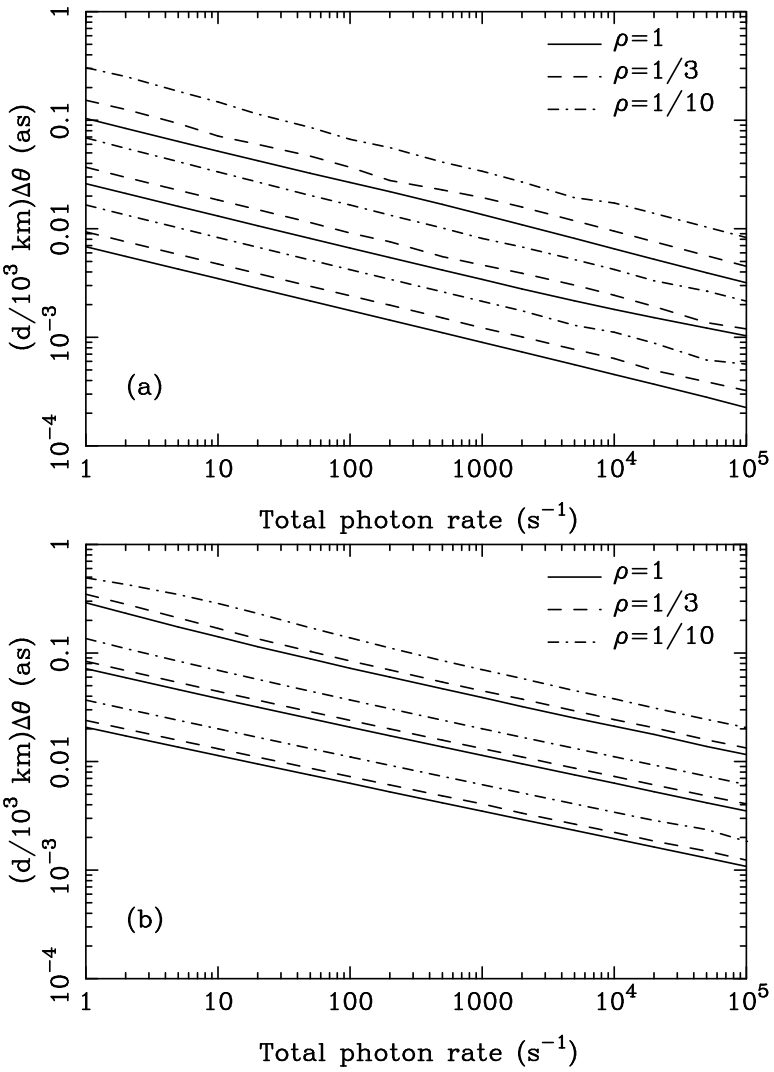

Figure 7: The minimum angular separation of two X-ray sources resolvable at the 95 percent confidence level. The limits are shown for intensity ratios, $\rho = 1$ (solid), $1/3$ (dashed), and $1/10$ (dashed-dotted). The upper set of three curves are for $\mu_\perp = 10$ mas s^{-1}, the middle set of three curves are for $\mu_\perp = 1$ mas s^{-1}, and the lower set of three curves are for $\mu_\perp = 0.1$ mas s^{-1}. Note that the total photon rate is of photons from the two sources detected in the telescope (without the presence *SOXS*), not photons incident on the telescope. Here d is the distance between the telescope and *SOXS* in units of 10^3 km. Panel (a) assumes no background whereas (b) has background equal to the flux of the two sources (so twice as many photons would be detected).

7.2 Elliptic Earth Orbits

We consider placing an *SOXS* in orbit around the Earth with nearly the same orbital parameters as an X-ray telescope. As discussed in section 2.2 we then allow for small alterations in the *SOXS* orbit which change the direction of the line-of-sight from the telescope to *SOXS* while keeping the *SOXS* period fixed. Our first constraint is that the minimum separation of the *SOXS* and telescope in their orbits must be larger than $10\ \mathrm{km}$. (If this safety factor can be reduced then greater sky coverage may be possible.) We then follow the two spacecrafts in their orbits to see what sky coverage these orbits afford. To limit the expenditure of propellant we consider making observations only when the relative velocity of the two satellites perpendicular to the line-of-sight is sufficiently small, here we require $v_{\perp}^{\mathrm{orb}} < 10\ \mathrm{m\ s^{-1}}$ (see section 4). Prior to an observation this velocity can be reduced to the desired range by firing the *SOXS* rockets (a small correction requiring acceptable use of consumables). Of course when we cancel $v_{\perp}^{\mathrm{orb}}$ before the observation we are also making a small change to the orbit.

The sky coverage on each change of *SOXS* orbit is not large. To increase the amount of sky accessible to observation we consider moving *SOXS* between orbits that are similar to the orbit of the X-ray telescope. Throughout we will consider modifications of the *SOXS* orbit that leave the period unchanged. Over many orbits this is a desired feature since it prevents the times at which *SOXS* and the telescope achieve apogee and perigee from drifting apart, requiring a large expenditure of fuel to correct. The orbital modifications we consider are increasing or decreasing the apogee distance (while preserving the semi-major axis and thus the period), rotating the orbit about all three axes, and introducing a phase shift (time of apogee) into the orbit. For this study we have considered both the *Chandra* and *XMM* X-ray telescopes and have allowed changes in apogee (and perigee) of $\pm 200\ \mathrm{km}$, rotations about the two axes in the plane of the orbit of $\pm 1^{\circ}$, rotations in the plane of the orbit of $\pm 0.4^{\circ}$, and time shifts of $\pm 100\ \mathrm{s}$. All of these changes are relative to the X-ray telescope's orbit. These changes can be accomplished using ion engines several thousand times before exhausting the supply of expendables (see section 4).

Using Monte Carlo techniques, we studied the orbits in this region of parameter space subject to two constraints: the minimum separation of the *SOXS* and telescope must be at least $10\ \mathrm{km}$, and somewhere in the orbit the perpendicular velocity must be less than $10\ \mathrm{m\ s^{-1}}$. We generated $100,000$ orbits that satisfy these criteria. Next, for a variety of photon count rates and desired resolutions we used the resolution results show in figure (7) to determine $\mu_{\perp}^{\mathrm{max}}$. Finally we checked which lines-of-sight satisfied velocity and acceleration constraints that guarantee a sufficiently long transit time across the source. The results are shown in figure 8 assuming the width of *SOXS* is $2\ \mathrm{m}$. Here $\Delta\theta$ is defined to be the minimum angular separation of two point sources that can be resolved at the 95 percent confidence level. For intense sources, $\Gamma = 10^5\ \mathrm{s^{-1}}$, with *Chandra* (a) we can obtain $\Delta\theta = 0.1\ \mathrm{arcsecond}$ over 40 percent of the sky and $\Delta\theta = 0.02\ \mathrm{arcsecond}$ over 10 percent of the sky. Similarly for *XMM* (b) we can obtain $\Delta\theta = 0.1\ \mathrm{arcsecond}$ for intense sources over 30 percent of the sky and have little sky coverage for $\Delta\theta < 0.04\ \mathrm{arcsecond}$.

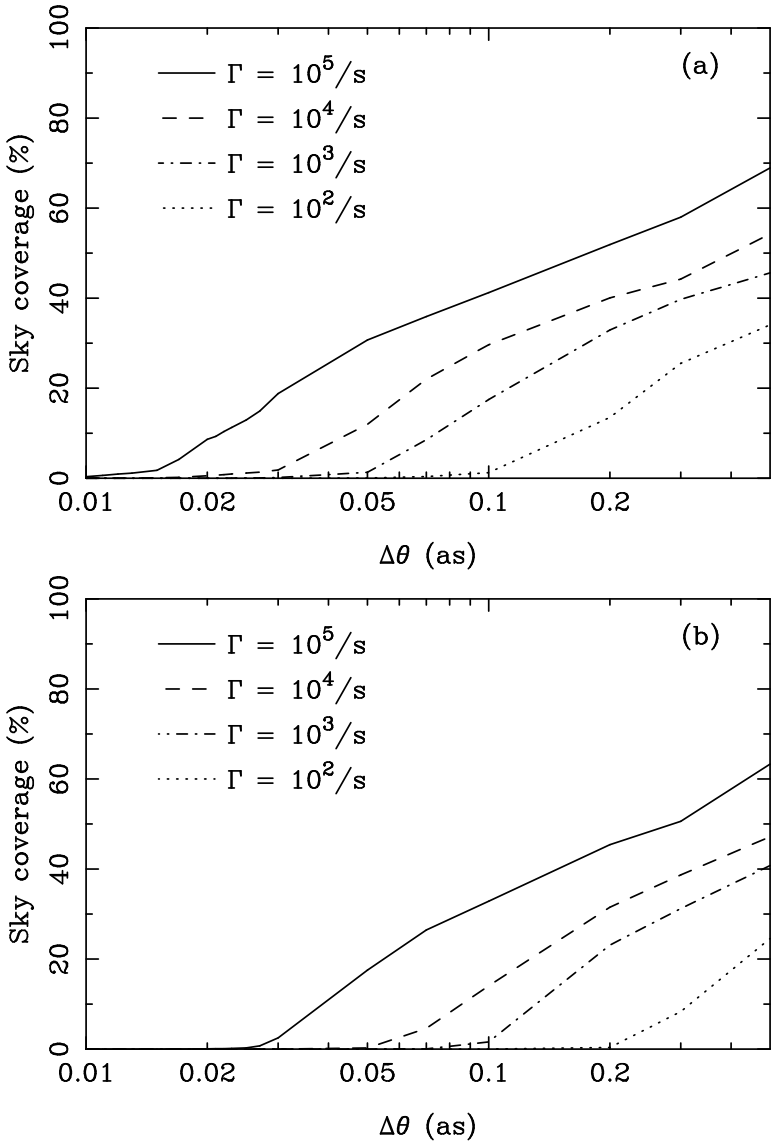

Figure 8: The fraction of the sky that can be observed as a function of the desired binary point source resolution, $\Delta\theta$, and the photon rate in the detector (as in figure 7b), Γ, for 2 m wide *SOXS*in conjunction with (a) *Chandra* and (b) *XMM*.

Table 1: Properties of existing and planned X-ray telescopes.

Satellite Name	Effective Area at 1 keV (cm^2)	Angular Resolution (arcsecond)	Orbit
Chandra (*AXAF*)[a]	700	0.5	eccentric high Earth orbit
XMM	2,000	15	eccentric high Earth orbit
Astro-E	1,200	90	low Earth orbit
HETE-II[b]	350	660	low Earth orbit
Constellation X	15,000[c]	15	L2 halo orbit
Xeus – Phase I	60,000	2	low Earth orbit
– Phase II	300,000	2	low Earth orbit

References:
Chandra: http://asc.harvard.edu/
XMM: http://xmm.vilspa.esa.es/
HETE-II: http://space.mit.edu/HETE/
Astro-E: http://heasarc.gsfc.nasa.gov/docs/astroe/overview.html
Constellation X: http://constellation.gsfc.nasa.gov/
Xeus: http://astro.estec.esa.nl/SA-general/Projects/XEUS/web/mission.html

[a] Effective area is for the *AXAF* CCD Imaging Spectrometer (ACIS). Angular resolution is for the High Resolution Camera (HRC).

[b] These values are for the wide field X-ray monitor (WXM) instrument. The quoted effective area is for 2 keV X-rays.

[c] Total effective area for all modules.

Larger sky coverages would be obtained if we relaxed the criteria on the orbital velocity difference between the X-ray telescope and *SOXS* orbits. This would be justified if the propellant velocities of ion engines rose about 30 $\mathrm{km\ s^{-1}}$, or if we could make do with a smaller number of orbital corrections.

8 Results

This is an exciting time for X-ray astronomy. Two new X-ray telescopes (the *Chandra Advanced X-ray Astronomical Facility*, and the *X-ray Multiple Mirror* telescope (*XMM*)) have been successfully launched, while another (*Astro-E*) is being readied for launch. Of these three, *Chandra* and *XMM* are in highly elliptical high altitude earth orbits (cf. Table 1) while *Astro-E* is headed for a circular low earth orbit. In addition, at least two major X-ray space-observatories are being planned: *Constellation X*, with launch scheduled for 2007, and *XEUS* with a target date of 2007. *Constellation X* will be placed at the L2 point of the Earth-Sun system, while *XEUS*, like *Astro-E*, will be placed in low Earth orbit.

While this may seem a remarkable proliferation of X-ray telescopes, each mission

has its own emphasis. In building an X-ray telescope there is a direct competition between large effective area (and thus sensitivity) and small acceptance angle (and thus high angular resolution). Therefore one must choose whether to build an instrument which aims for high angular-resolution or one which has a goal of achieving high sensitivity. *Chandra* is the only high angular resolution instrument of the listed missions, with a maximum resolution of 0.5 arcsecond and thus has the relatively small effective area given above (13). The other instruments all aim for large effective area, and so sacrifice angular resolution. *XMM*, which is already flying, has considerably larger effective area than *Chandra* (and thus much lower angular resolution). *Astro-E* will have even larger effective area. *Constellation X* will consist of multiple X-ray telescopes flown in formation, with a total effective area considerably greater than either *XMM* or *Astro-E*; it too has relatively low angular resolution compared to *Chandra*. Finally *XEUS* will have a huge effective area, and will be designed to be expandable. Its angular resolution is better than *XMM*, *Astro-E*, or *Constellation X* but still not as good as *Chandra*. The properties of the existing and planned telescopes are shown in Table 1.

Throughout we have considered the photon rate in the detector, not at the surface of the telescope. An X-ray telescope has an effective area, $\mathcal{A}$, which includes the geometric collecting area (since grazing optics are used the collecting area is not the full beam) and the efficiency of the X-ray detector. As an example, with *Chandra*

$$\mathcal{A}_{Chandra} \approx 700 \text{ cm}^2 \tag{13}$$

for $E \approx 1$ keV. This is the area to be used as the area of the telescope, not the geometric area as in the case of optical telescopes. The effective area for existing and planned X-ray telescopes is given in Table 1.

The luminosity of X-ray sources varies greatly. Black holes in the cores of nearby galaxies have

$$\mathcal{L}_{\rm bh} \approx 10^{38-40} \text{ erg s}^{-1} = 6.2 \times 10^{46-48} \text{ keV s}^{-1} \tag{14}$$

in the 0.2–2.4 keV energy range. This leads to a photon rate at the surface of the detector of

$$\Gamma_{\rm bh} = 6.5 \times 10^{0-2} \left(\frac{E}{\text{keV}}\right) \left(\frac{d}{1 \text{ Mpc}}\right)^{-2} \left(\frac{\mathcal{A}}{1000 \text{ cm}^2}\right) \text{ s}^{-1}, \tag{15}$$

where the energy, E, we observe at is given in keV and $\mathcal{A}$ is the effective area of the X-ray telescope as discussed above.

An active galactic nucleus (AGN), Seyfert galaxy, or the core of X-ray clusters can be much more luminous

$$\mathcal{L}_{\rm AGN} \approx 10^{40-44} \text{ erg s}^{-1} = 6.2 \times 10^{48-52} \text{ keV s}^{-1}. \tag{16}$$

However, since they are approximately 100 Mpc away the photon rate is only

$$\Gamma_{\rm AGN} = 6.5 \times (10^{-2}\text{–}10^{2}) \left(\frac{E}{\text{keV}}\right) \left(\frac{d}{100 \text{ Mpc}}\right)^{-2} \left(\frac{\mathcal{A}}{1000 \text{ cm}^2}\right) \text{ s}^{-1}. \tag{17}$$

Galactic microquasars are somewhat less luminous

$$\mathcal{L}_{\rm microquasar} \approx 10^{39}\ {\rm erg\ s^{-1}} = 6.2 \times 10^{47}\ {\rm keV\ s^{-1}}, \tag{18}$$

since they are in our own galaxy, though, the photon rate is fairly high

$$\Gamma_{\rm microquasar} = 6.5 \times 10^{5} \left(\frac{E}{\rm keV}\right) \left(\frac{d}{10\ {\rm kpc}}\right)^{-2} \left(\frac{\mathcal{A}}{1000\ {\rm cm^2}}\right)\ {\rm s^{-1}}. \tag{19}$$

For a $2\ {\rm m}$ *SOXS* employed in conjunction with *Chandra* we find (figure 8a) that for the brightest sources we can obtain $\Delta\theta = 0.5\ {\rm arcsecond}$ over about 50 percent of the sky, $\Delta\theta = 0.1\ {\rm arcsecond}$ over about 20 percent of the sky, and $\Delta\theta = 0.05\ {\rm arcsecond}$ over about 5 percent of the sky. Thus significant improvements are attainable through the use of an *SOXS* with *Chandra*.

For an *SOXS* employed in conjunction with *XMM* the situation is similar. Although *XMM* has a shorter period than *Chandra* its has an effective area about 3 times larger (Table 1). Still *Chandra* provides superior results. Note that tremendous improvements over the nominal $15\ {\rm arcsecond}$ resolution for *XMM* are obtained with the aid of *SOXS*.

At L2 the situation is even better. Since we can tune the velocity relative to the line-of-sight more easily, great improvements in resolution are readily available (figure 7). Sub-milliarcsecond resolution can be obtained for sources with photon rates $\Gamma \gtrsim 1000\ {\rm s^{-1}}$. For a single *Constellation X* modules, which will have an effective area of about $15,000\ {\rm cm^2}$, the brightest AGN's, X-ray cluster cores, and galactic black holes will have $\Gamma \approx 800\ {\rm s^{-1}}$ we can obtain $\Delta\theta \approx 2\ {\rm mas}$.

9 Conclusions and Future Work

We have found that an *SOXS* used in conjunction with an X-ray telescope can lead to tremendous improvements in angular resolution. The trend of increasing the effective area of future X-ray telescopes at the expense of angular resolution (Table 1) meshes perfectly with the benefits gained by including an *SOXS* in the mission. Indeed, an X-ray telescope to be used with an *SOXS* is treated as a light bucket with all the resolving power coming from the *SOXS* occulting the source. Thus an *SOXS* is an excellent addition to an X-ray telescope mission, particularly one at L2, such as *Constellation X* where sub-milliarcsecond resolution can be attained for a wide range of sources.

For the *Chandra* X-ray telescope we found that moderate improvements in angular resolution over an appreciable fraction of the sky can be achieved through the use of an *SOXS*. Similarly an *SOXS* employed in conjunction with *XMM* would provide tremendous improvements in the angular resolution that *XMM* could achieve allowing *XMM* to have angular resolution comparable to *Chandra*. An *SOXS* launched for use with *Chandra* or *XMM* would also provide an important test bed for the technology to be used with future missions.

Much work remains, however, to be done. In particular:

- While we have successfully demonstrated the ability to reconstruct complex compound images from occultation data, our reconstruction scheme is far from optimal. (While the problem sounded straightforward, it proved to be in a different domain of image reconstruction parameter space than others have usually worked in.) We are therefore currently underestimating the reconstructive potential of our technique.
- The link between test images and scientific targets is still inadequate. The issue has been that there do not exist such high resolution simulated images of X-ray sources, probably because researchers have not been motivated by data, or promises of data, to produce them.
- We have not optimized the occulting mask. A simple square clearly does not maximize the possible information per transit. Techniques developed in standard X-ray imaging (coded masks) may offer a very attractive (even rigorously optimizable) solution.
- We have not adequately explored the positioning/attitude/orientation control problem which must be solved in order to provide the desired very long-lasting slow transits of the occulter across the line of sight.
- We have not faced the design issues of how to build, launch, deploy and manuever such an occulter.

These are the tasks we will propose to confront in Phase II. We believe the results of the Phase I study suggest that continued investigation of the steerable X-ray occulting satellite concept is merited.

References

[1] Adams, D.J. et al., 1988, *The Astrophysical Journal*, 327, L65

[2] Baptista, R. & Steiner, J.E., 1991, *Astronomy and Astrophysics*, 249, 284

[3] Baptista, R. & Steiner, J.E., 1993, *Astronomy and Astrophysics*, 277, 331

[4] Copi, C.J. & Starkman, G.D., 1998, Proceedings of SPIE, 3356, March 25, 1998, Kona, HI

[5] Copi, C.J. & Starkman, G.D., 2000, *The Astrophysical Journal*, 532, 581

[6] Copi, C.J. & Starkman, G.D., American Astronomical Society Meeting 197, #49.06.

[7] Schneider, J., 1995, Proceeding of the workshop "Detection and Study of Terrestrial Extra-solar Planets", May 15–17, Boulder, CO, unpublished